Photophysical Ion Dynamics in Hybrid Perovskite MAPbX3 (X=Br, Cl) Single Crystals

RESEARCH ARTICLE

Editor's Choice

ADVANCED PHYSICS RESEARCH Open Access

www.advphysicsres.com

Photophysical Ion Dynamics in Hybrid Perovskite $MAPbX_3$ (X=Br, Cl) Single Crystals

Konstantinos Papadopoulos, Ola Kenji Forslund,* Stephen Cottrell, Koji Yokoyama, Pabitra K. Nayak, Francoise M. Amombo Noa, Lars Öhrström, Elisabetta Nocerino, Lars Börjesson, Jun Sugiyama, Martin Månsson, and Yasmine Sassa**

Hybrid organic–inorganic perovskites (HOIPs) are promising candidates for next-generation photovoltaic materials. However, there is a debate regarding the impact of interactions between the organic center and the surrounding inorganic cage on the solar cell's high diffusion lengths. It remains unclear whether the diffusion mechanism is consistent across various halide perovskite families and how light illumination affects carrier lifetimes. The focus is on ion kinetics of $(CH_3NH_3)PbX_3$ (X = Br, Cl) perovskite halide single crystals. Muon spectroscopy (μ^+SR)is employed to investigate the fluctuations and diffusion of ions via the relaxation of muon spins in local nuclear field environments. Within a temperature range of 30–340 K, ion kinetics are studied with and without white-light illumination. The results show a temperature shift of the tetragonal-orthorhombic phase transition on the illuminated samples, as an effect of increased organic molecule fluctuations. This relation is supported by density functional theory (DFT) calculations along the reduction of the nuclear field distribution width between the phase transitions. The analysis shows that, depending on the halide ion, the motional narrowing from H and N nuclear moments represents the molecular fluctuations. The results demonstrate the importance of the halide ion and the effect of illumination on the compound's structural stability and electronic properties.

1. Introduction

In the pursuit of global environmental restoration, extensive endeavors have been undertaken to harness the sun's energy, since the first practical silicon solar cell was introduced in 1954.[1] Presently, most investigations are primarily centered on the enhancement of solar cell efficiencies, with the concurrent objective of utilizing materials that are abundant on our planet. In this regard, HOIPs have been found to effectively fulfill most objectives.[2] The power conversion efficiency of hybrid perovskite solar cells has been shown to reach 26.1%, rivalling crystalline silicon cells.[3,4] Given the prerequisite that they are produced in an environmentally friendly manner, and that the assembly of a functional perovskite cell is as straightforward as positioning the perovskite absorber between an electron transport layer and a hole transport layer, perovskite solar cells appear to possess considerable promise for fostering sustainable growth.[2,5]

K. Papadopoulos, L. Börjesson, Y. Sassa
Department of Physics
Chalmers University of Technology
Göteborg SE-41296, Sweden
E-mail: konpap@chalmers.se; sassa@kth.se

O. K. Forslund
Physik-Institut
Universität Zürich
Winterthurerstrasse 190, Zürich CH-8057, Switzerland
E-mail: ola.forslund@physik.uzh.ch

The ORCID identification number(s) for the author(s) of this article can be found under https://doi.org/10.1002/apxr.202300120

DOI: 10.1002/apxr.202300120

O. K. Forslund
Department of Physics and Astronomy
Uppsala University
Box 516, Uppsala SE-75120, Sweden

S. Cottrell, K. Yokoyama
ISIS Pulsed Neutron and Muon Facility
STFC Rutherford Appleton Laboratory
Didcot, Oxfordshire OX11 0QX, UK

P. K. Nayak
Tata Institute of Fundamental Research 36/P
Gopanpally Village, Hyderabad 500046, India

F. M. A. Noa, L. Öhrström
Department of Chemistry and Chemical Engineering
Chalmers University of Technology
Gothenburg SE-41296, Sweden

E. Nocerino
Department of Materials and Environmental Chemistry
Stockholm University
Stockholm 106 91, Sweden

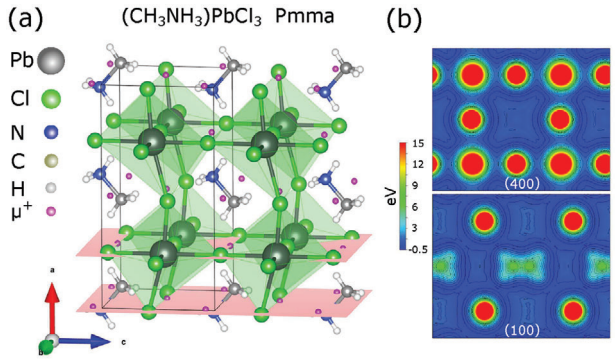

Figure 1. Example of the orthorhombic crystal structure of $MAPbX_3$ (X = Cl, Br) and electrostatic potential calculation for determining the muon implantation sites. a) The orthorhombic crystal perovskite structure of $MAPbCl_3$, including (b) the probable locations of implanted muons. These probable muon sites were determined from the minima of electrostatic potential calculations. Intersections of the charge density in the lattice planes (100) and (400) present the possible muon sites (pink color).

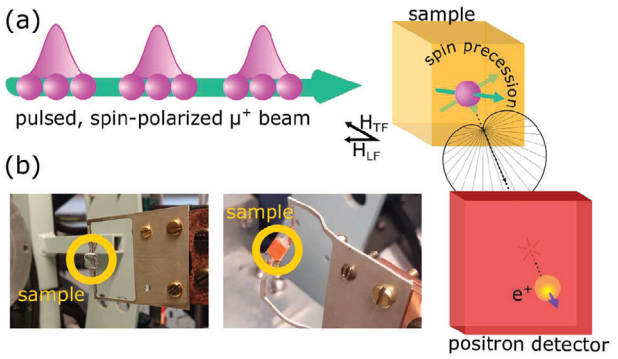

Figure 2. Illustration of the μ^+SR set-up featuring the mounting of the HOIP crystals $MAPbX_3$ (X = Cl, Br). a) Schematic of the μ^+SR experiment in EMU, ISIS. A spin polarized, pulsed muon beam hits the sample. The positive muons are implanted at electrostatically preferable lattice sites and their spin precesses as affected by surrounding local magnetic fields. Following each muon decay, the emitted positrons with momentum direction statistically along the muon spins reach the surrounding detectors. The evolution of muon spin precession can be studied from the ensemble of detected positrons. b) Pictures of the sample holders used for the dark and light on/off experiments. In the light on/off experiment, the sample holder is bent to 45° for the sample to be subjected to both light and the muon beam.

The HOIP crystals in question are a form of the ABX_3 single perovskite structure.[6] They are composed of a methylammonium (MA) organic cation $(CH_3NH_3)^+$ at the A-site, a Pb^{2+} cation at the B-site, and a halogen anion, Br^- or Cl^-, at the X-site, as illustrated in **Figure 1a**. The MA molecule sits in the center of a framework with edge-sharing PbX_6 octahedra. Both $MAPbBr_3$ and $MAPbCl_3$ crystallize in the cubic $Pm3m$ system at room temperature.[7] The Br crystal undergoes two structural transitions, one at ≈230 K from cubic to tetragonal and one at ≈144 K from tetragonal to orthorhombic (see Table S2.1, Supporting Information). An additional phase transition appears at ≈150 K, which has been assigned to an incommensurate crystal phase formed by the organic–inorganic coupling.[8–10] For the Cl crystal the same structural transitions occur at ≈175 and ≈169 K (see Table S2.1, Supporting Information), respectively.[11]

The halogen anions are highly electro-negative, enhancing the ionicity of the perovskite. The semiconducting properties arise from the inorganic structure and by exchanging or mixing the halogen ions, one can tune the bandgap energy to tailor the material for specific applications.[12] The reported bandgap values for $MAPbBr_3$ and $MAPbCl_3$ are 2.39 and 3.16 eV respectively, making them sensitive to visible and ultraviolet light.[13,14] Their carrier lifetimes, as determined by photoluminescence and transient absorption spectroscopy,[15–19] cover the nano- to microsecond time scale, revealing fast, and slow carrier dynamics. The rotating organic cations play a crucial role in determining the structure and the stability of the crystal. These organic molecules form permanent dipoles that can be frozen in space or possess rotational degrees of freedom, which can be observed on the picosecond time scale, with or without intersite correlations.[20] These molecular fluctuations may drive the formation of polarons that create a dynamic screening to the charge carriers. This is the most likely scenario put forward to explain the long carrier lifetimes in $MAPbX_3$.[21,22]

μ^+SR is a well established microscopic technique in the study of ion kinetics.[23,24] A recent μ^+SR study reported the ion diffusion in the archetypal halide perovskite $MAPbI_3$.[25] Although their results demonstrate a relation between the rotation of the electric dipoles of MA molecules and the charge carrier lifetime in $MAPbI_3$, it remains ambiguous if a similar mechanism can be extended to other halide perovskite solar cell compounds. Furthermore, their study has been conducted on $MAPbI_3$ powder sample, giving an average of the diffusion length among multiple directions and influenced by grain boundaries.[26] Finally, their measurement does not consider the effect of illumination, which can drastically influence the dynamics of ions.

Here, we employ μ^+SR with a pulsed muon source (**Figure 2a**) to study the ion dynamics in $MAPbX_3$ (X = Cl, Br) single crystals as a function of temperature, with and without white light illumination (see Experimental Section). Contrary to powder samples, single crystals present the advantage of studying the ion diffusion along specific directions[27] and present an ideal platform in the development of optoelectronic devices. Through our measurements we extract the evolution of the internal nuclear magnetic field distributions of the involved ions over a temperature range of 30 − 340 K. The fluctuation rate of the field distribution is a direct measure of the dynamics of the ionic species. Using muon as a local probe with well-defined implantation sites and a wide time window of 10^{-5}–10^{-11} s, gives spatially specific information on the muon-lattice dynamics. Both static and dynamic contributions to the muon spin depolarization are identified and evaluated. Our results show that, depending on the halide ion and the local conditions (e.g., with or without light), the motional narrowing from H and N nuclear moments has an impact on the structure stability and the charge carrier lifetimes.

2. Results

Zero field (ZF), longitudinal field (LF), and transverse field (TF) μ^+SR measurements were conducted in illuminated and dark environment (Figures 2 and 3) to characterize the local nuclear magnetic field distributions as a function of temperature.[24,28] During

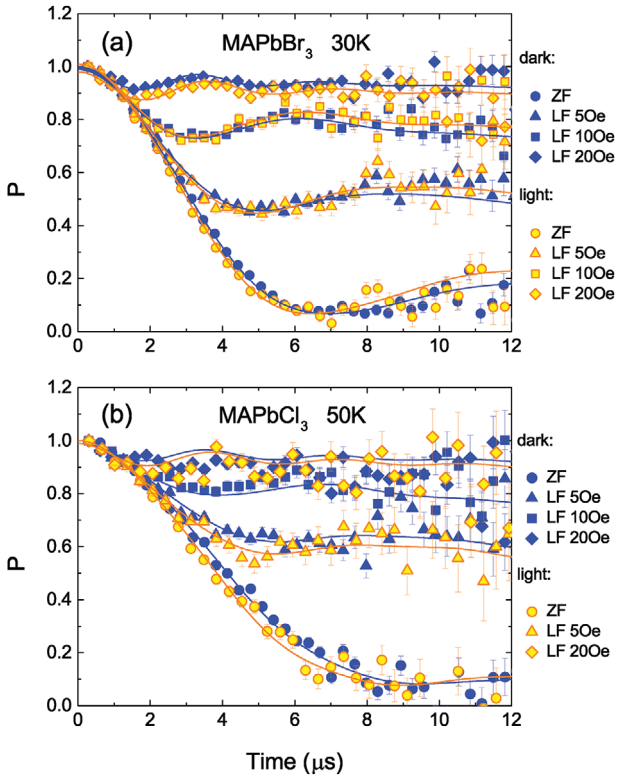

Figure 3. ZF and LF μ^+SR depolarization spectra of $MAPbBr_3$ and $MAPbCl_3$ in a dark and illuminated environment. The ZF and LF= 5, 10, 20 Oe time spectra are recorded at a) $T = 30$ K for $MAPbBr_3$ and b) $T = 50$ K for $MAPbCl_3$, in the dark condition and under illumination. The solid lines are fits obtained from Equation (1).

the illuminated measurements the depolarization in the consecutive light on/off periods (see Experimental Section) were identical (see Section S.3, Supporting Information), indicating that photo-induced ion dynamics were sustained through the light-off cycle. In contrast, the depolarization in the constant dark configuration, produced effectively different results.

2.1. $(CH_3NH_3)PbBr_3$

The ZF and LF time spectra for $MAPbBr_3$, collected at $T = 30$ K in the dark condition or under illumination, are shown in Figure 3 with subtracted background asymmetries and normalized. A Gaussian Kubo-Toyabe (KT)-like relaxation[24,29] is observed together with a small offset. Therefore, the time spectra were fitted using dynamic Gaussian-KT together with a non-relaxing component:

$$A_0\, P_{LF}(t) = A_{KT}\, G^{KT}(H_{LF}, \Delta_{KT}, \nu_{KT}, t) + A_{BG} \quad (1)$$

where A_0 is the initial asymmetry whose values depend on the instrument, while P_{LF} is the polarisation function under ZF and LF configurations. A_{KT} and A_{BG} are the asymmetry of each contribution to the muon depolarization and correspond to the volume fraction of the measured sample. The KT parameters, Δ_{KT} and ν_{KT}, are the field distribution width and the field fluctuation rate.[29] Since weak LF is able to decouple the muon spin from the static intrinsic fields (Figure 3a), the randomly oriented internal field is expected to originate from $I_H = 1/2$, $I_N = 1$, $I_{Pb} = 1/2$ and $I_{Br} = 3/2$ nuclear moments.

Weak LF is not expected to affect the spin–spin correlation times in the system and the KT parameters were fitted as common parameters across the different field configurations. Moreover, A_{BG} was kept fixed across the temperature range, a value estimated at a low temperature measurement for which the internal magnetic field of the sample is shown to be static. The obtained KT fit parameters from Equation (1), under these conditions, are shown in **Figure** 4a,b as a function of temperature. At low temperatures, no significant difference is observed between light and dark measurements. Below 140 K, Δ_{KT} poses a constant value of about $\approx 0.28\ \mu s^{-1}$. This value is consistent with the expected value considering a muon situated at fractional coordinates (0.22, 0.25, 0.25) in the orthorhombic cell, for which $\Delta^{ortho} \approx 0.298\ \mu s^{-1}$ using the powder average expression in the Van Vleck formalism.[30,31] The sudden decrease around $T_{C1}^{Br} = 145$ K is consistent with the incommensurate phase transition,[8,32,33] evidence of which were found in X-ray diffraction with the appearance of satellite peaks at various fraction positions around the unit cell sites, as well as an additional heat flow peak in DSC measurements (see Figure S1.1, Supporting Information).

The structural transitions change the nuclear coupling between lattice and muons and a new value of $\Delta_{KT} \approx 0.12\ \mu s^{-1}$ is stabilised in the tetragonal phase. Another drop is observed around $T_{C2}^{Br} = 220$ K, which subsequently infers a structural transition from tetragonal to cubic symmetry.[10,32] It is not unexpected that these structural transitions are present in both dark and light configurations as inferred from Figure 4b. It is evident that the nuclear coupling under new symmetry cannot solely explain the magnitude of the drop in Δ_{KT}, since there is a large difference between the calculated (solid red lines) and experimental values. The drop can however be explained by introducing dynamics and is thereupon related to the local field fluctuation rate (ν_{KT}). We present ν_{KT} as a function of temperature in Figure 4a. An exponential-like increase is observed from lower temperatures and up to about T_{C1}^{Br}. This increase resembles an Arrhenius activation, and the calculated activation energies are tabulated in Table 2. Additionally, the corresponding fits are presented in the Figure S3.3 (Supporting Information). A second increase is observed approaching T_{C2}^{Br}. The value and behavior of ν_{KT} is similar to what was observed for $MAPbI_3$.[34] Past μ^+SR work on $MAPbI_3$ suggested this increase to stem from fluctuations caused by the rotations of the MA molecule.[25,34] Consequently, the decrease observed just above T_{C1}^{Br} was explained as motional narrowing associated to the dynamics of H atoms, and further increase of ν_{KT} at higher temperatures was asserted to be due to I diffusion. Given the resemblance in behavior of $MAPbBr_3$, it is naturally reasonable to assume that a similar mechanism is behind the obtained temperature dependence. However, the proposed scenario has not yet been validated.

In order to confirm the premise, we have calculated the expected internal field distribution widths Δ, at the muon sites, for their respective crystal symmetries. **Table** 1 summarizes the calculation results of the expected Δ, for each crystal symmetry, at the expected muon sites. The electrostatic potential minima

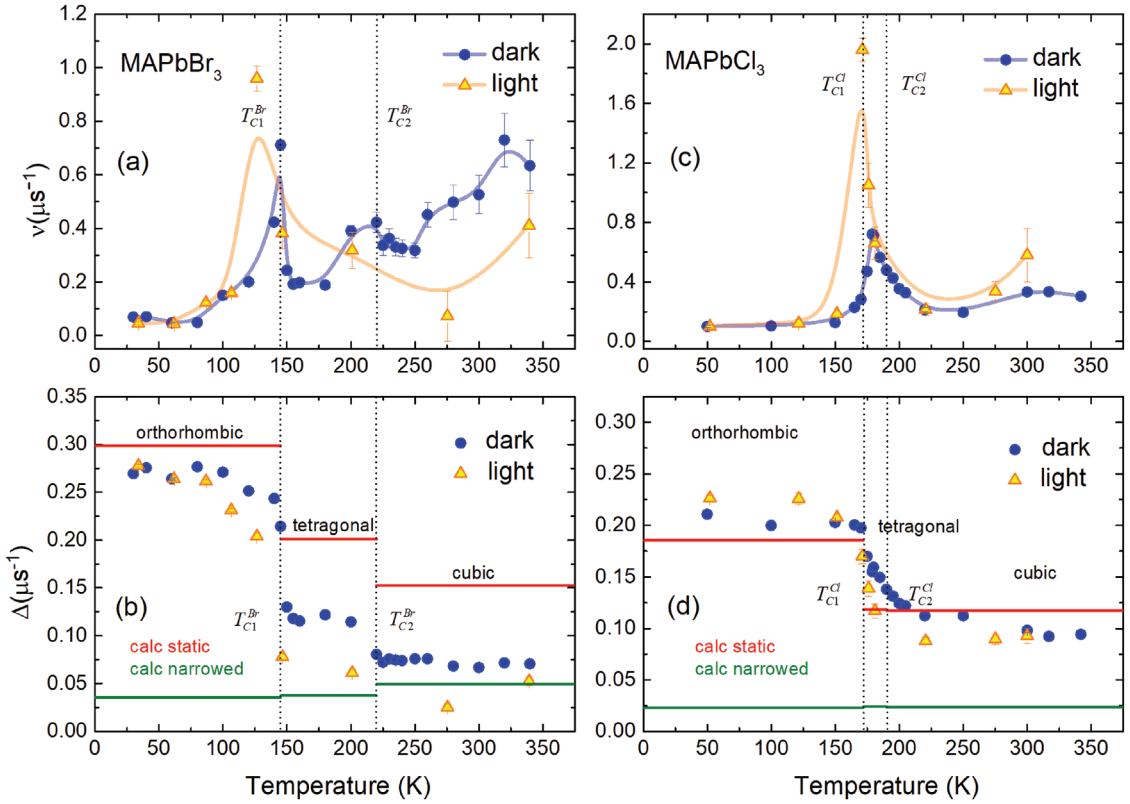

Figure 4. Fitting parameters from the $MAPbBr_3$ and $MAPbCl_3$ μ^+SR depolarization spectra. Temperature dependent a) field fluctuation rate (ν_{KT}) and b) field distribution width (Δ) of $MAPbBr_3$ in dark and illuminated configuration, obtained using Equation (1). Temperature dependent c) field fluctuation rate (ν_{KT}) and d) field distribution width (Δ) of $MAPbCl_3$ in dark and light configurations, obtained using Equation (1). The dashed lines mark the structural transition temperatures. The solid lines in (a,c) are a guide to the eye, while in (b,d) are the calculated values in the static and motionally narrowed case (see Table 1).

(Figure 1b) suggest two muon sites with fractional coordinates μ_1: (0.22, 0.25, 0.25) and μ_2: (0.0, 0.5, 0.5).

The results are shown as solid lines in Figure 4b. The agreement of the calculated values (Δ_{Br}^{static}) with the measured values in the orthorhombic phase confirms the μ_1 muon site determined via our method. However, mismatches are observed in tetragonal and cubic phases. In other words, the nuclear coupling under new symmetry cannot explain the total magnitude of the drop. In fact, the calculated value (calc. narrowed) sets a lower boundary to the measured value if H and N contributions are excluded from the calculation. This suggests that the field distributions associated to H and N nuclear moments are motionally narrowed[23,35] and is consistent with the scenario put forward in the past;[25,34] the drop in ν_{KT} at T_{C1}^{Br} is caused by motional narrowing associated to the MA cage. This scenario is also endorsed by the endothermic minima of the MDSC non-reversible component (see Figure S1.1, Supporting Information). An analysis using quasi-elastic neutron scattering[21] and nuclear magnetic resonance studies,[36–38] where the rotational freedom of the MA cage increases in the tetragonal and cubic phases compared to the orthorhombic phase, also supports this proposed framework. Therefore, we conclude that mainly Br nuclear moments contribute to the increase of ν_{KT} at higher temperatures. Interestingly, there is a large difference between dark and light configurations in ν_{KT} at low temperatures, and is further discussed below.

Table 1. Calculated local field distribution widths. The local field distribution widths (Δ_X^{static}, X = Cl and Br) for the respective muon sites, for each crystal symmetry, calculated in the Van Vleck limit. The value in which the MA cage is motionally narrowed ($\Delta_X^{narrowed}$) is also included.

Muon site	Δ_{Cl}^{static} [μs^{-1}]	$\Delta_{Cl}^{narrowed}$ [μs^{-1}]	Δ_{Br}^{static} [μs^{-1}]	$\Delta_{Br}^{narrowed}$ [μs^{-1}]
μ_1^{ortho}	0.185508	0.010777	0.298856	0.035615
μ_1^{tetra}	0.115962	0.010481	0.200948	0.037521
μ_1^{cubic}	0.117299	0.010587	0.152858	0.049387
μ_2^{ortho}	0.115822	0.023163	0.189069	0.069558
μ_2^{tetra}	0.118294	0.024104	0.289017	0.018813
μ_2^{cubic}	0.120129	0.023462	0.314969	0.045232

2.2. $(CH_3NH_3)PbCl_3$

The ZF and LF time spectra collected for $MAPbCl_3$ at T = 50 K are shown in Figure 3b. Similar to the X = Br compound, a KT and an offset signal is manifested in the time spectra. In this case, the KT signal is the effect due to I_H, I_N, I_{Pb}, and I_{Cl} = 3/2 nuclear moments. Equation (1) was used in order to fit the time spectra as a function of temperature, under the same conditions as described above and is shown in Figure 4c,d. Δ_{KT} shows a

Table 2. Calculated activation energies (E_a) for $MAPbBr_3$ and $MAPbCl_3$, below T_{C1}, in the dark and light environment. The references include E_a results in the same temperature range.

Sample	E_a^{dark}[meV]	E_a^{light}[meV]	Ref.
$MAPbBr_3$	37.2(9.7)	27.3(9.7)	[39–42]
$MAPbCl_3$	170.8(29.8)	105.4(81.5)	[40–44]

temperature independent behavior at low temperatures. The value $\approx 0.23\ \mu s^{-1}$ is in agreement with the expected local field value at the (0.22, 0.25, 0.25) muon site, in the orthorhombic phase. We should however note that the main result presented here is not dependent on the specific muon site. Regardless, Δ_{KT} experiences a sudden drop around $T_{C1}^{Cl} = 172$ K, which is consistent with a structural transition temperature.[11] Once again, this transition changes the nuclear coupling with the muons. Unlike the $X =$ Br compound, Δ_{KT} is not stabilized onto another value but a continuous decrease is observed in the tetragonal phase. The origin is discussed later on. A final structural transition is present around $T_{C2}^{Cl} = 190$ K and results in a second drop of Δ_{KT}, which stabilizes at a value $\Delta_{KT} \approx 0.1\ \mu s^{-1}$. These structural transitions are present in both light and dark configuration.

The local field fluctuations rate, ν_{KT}, is shown in Figure 4c. An exponential like increase is observed at lower temperature up to T_{C1}^{Cl}. The Arrhenius fits are presented in the Figure S3.3 (Supporting Information) and the activation energies for both the light and dark environment are documented in **Table 2**. The E_a values decrease with illumination, but increase with halide substitution depending on ionic size and hydrogen bonding strength, as reported in previous studies. As already mentioned, a similar increase in ν was observed in $MAPbI_3$[25,34] and was previously speculated to be due to fluctuations from the MA molecule, for which the sudden decrease was explained by motional narrowing from H moments. Similar to the $X =$ Br sample, the increased dynamics are indicated by the DSC non-reversible heat flow component (see Figure S1.1, Supporting Information). We have calculated the local field arising from nuclear moments at the muon sites in their respective crystal symmetries, to support this assessment.

The results of our calculations for each crystal symmetry are presented in Table 1 and are shown as solid lines in Figure 4d. Once again, the calculated static value is comparable with the experimental values in the orthorhombic phase. However, in the $(CH_3NH_3)PbCl_3$ case the static calculations continue to produce a better fit for the tetragonal and cubic phases in contrast to excluding H and N contributions. It is expected that the lighter and more electronegative Cl will form stronger hydrogen bonds with the MA molecule, which as a result stabilizes the structure.[45–47] Mostly Cl nuclear moments are expected to contribute to the increase of ν at higher temperatures. The temperature dependence of ν_{KT} seems comparable between light and dark modes but differences are present at lower temperatures and the origin is discussed below.

3. Discussion

The analysis on muon depolarization spectra for $MAPbBr_3$ and $MAPbCl_3$ has confirmed the structural transitions[10,11] and given evidence of increasing MA^+ fluctuations and Br^-,Cl^- diffusion[48] as the crystal structure evolves from orthorhombic to tetragonal, to cubic crystal symmetry with increasing temperature. The calculated local field values for both static and motionally narrowed MA^+ are presented together with the experimental results. A similar framework was considered previously in the same and sister compounds.[21,34,49,50] In the $MAPbI_3$ compound, the temperature dependence of the field distribution width was shown to coincide with photoluminescence carrier lifetimes as a function of temperature.[25] Furthermore, MA^+ has a permanent electric dipole moment, the fluctuations of which result to an abrupt increase of the complex permittivity components at T_{C1}.[7,51] It is thus of high interest to study complex permittivity measurements at frequencies near the charge carrier lifetimes of those compounds[52] and determine possible correlations between charge carriers and MA^+.

The effect of illumination is indirectly observed but evident in the ν_{KT} and Δ_{KT} evolution with temperature. For both samples, the effect of the flash lamp is most prominent below T_{C1}, where MA cage fluctuations are initiated. In fact, the peak feature of ν_{KT} is shifted to lower temperature under illumination. Coincidentally, the sharp drop of Δ_{KT} seems to be occurring at lower temperature as well. This suggests that the structural transition taking place at T_{C1} is driven by MA motion, specifically C3 rotation. This assessment is in line with quasi-elastic neutron scattering measurements[21] in which the relaxation time of the rotational motion around the C3 axis seem to exhibit a plateau below T_{C1}.

A question remains however, why are the MA cage fluctuations affected by the illumination. From the presented data, it appears that illumination is enhancing the MA dynamics, as evidenced from the temperature shift of the lower peak and the increase of ν_{KT} in terms of absolute value. Recent studies proposed a relationship between carrier lifetime and MA fluctuations.[25,53,54] The long carrier life was ascribed to the dynamic motion of MA molecules, in which dynamic screening via formation of polarons protects the carriers. It is currently believed that the MA dynamics is driving the formation of polarons and thus increasing the lifetime of the carriers.[22,55] Our results suggest that these effects appear in symbioses. By exciting electrons and inducing electron carriers, the dynamics of the MA cage is enhanced and is likely resulting in the formation of polarons.

The high temperature behavior of ν_{KT} was ascribed to Br and Cl dynamics, respectively. For the $X =$ Cl sample no significant difference is observed between dark and light configuration. Similarly, the $X =$ Br sample does not show any large differences. While we cannot fully exclude the possibility of diffusing muons above 150 K, future negative μ^-SR measurements can experimentally determine the diffusing species.[56] One may argue that the Br diffusion is lower in light configuration. However, the number of measurement points need to be increased in order to further comment on the origins or the validity of this effect. With that said, it has been suggested that electronic carrier diffusion can either enhance or suppress ionic diffusion through ambipolar transport.[57] Also, we should note that the efficiency of solar cells can be improved by restricting the diffusion of these ions. In fact, partial substitution of I with Br[49] showed that the activation energy of I diffusion increases. In other words, partial cation substitution may restrict

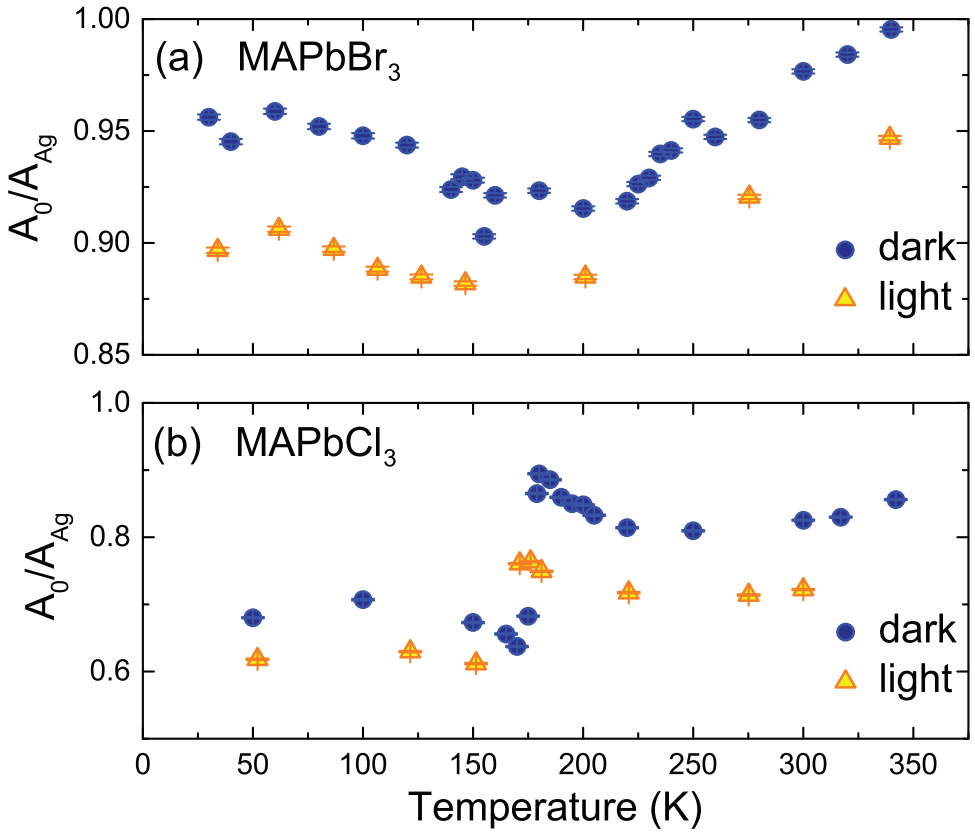

Figure 5. The initial asymmetry of $MAPbBr_3$ and $MAPbCl_3$ with and without illumination. The initial asymmetry (A_0), estimated in TF configuration for a) $MAPbBr_3$ and b) $MAPbCl_3$ in the dark and light configurations.

the diffusive behavior and thus increase the overall solar cell performance.

The diagmagnetic sample fraction is estimated from the TF precesion amplitude (**Figure 5**). Its temperature dependence is observed in the initial TF asymmetry (A_0), in good agreement with previous dielectric studies.[7,51] The residual missing fraction probably originates from muonium typically formed in semiconducting/insulating materials because of the lack of electron screening.[58–61] A muonium quasi-atom is formed when a μ^+ captures an e^-. The capture cross section is inversely proportional to the dielectric constant, which can explain why the muonium formation is more prominent in $MAPbCl_3$.[62] With this in mind, we would like to conclude with a last remark on the possibility of monitoring hydrogen kinematics through the study of muoniums. Recently, it was reported that highly diffusive H^+ impurities are present in $MAPbI_3$,[63] hampering the solar cell's performance. This is a common issue with semiconducting materials, where μ^+SR has been successfully employed to further our understanding on the fundamental aspects of hydrogen kinematics.[64,65]

4. Conclusion

The current study presented μ^+SR measurements on single crystal, HOIPs $MAPbX_3$ (X = Br, Cl), in which the static and dynamic changes of internal, nuclear magnetic fields were measured as a function of temperature and magnetic field. At low temperatures, the onset of MA molecule fluctuations is found to drive the orthorhombic/tetragonal structural transition. The presented data suggest Cl^- and Br^- diffusion to take place at high temperatures. By illuminating the sample, the number of excited carriers can be increased. This has an effect on the lattice dynamics of these systems as the MA cage dynamics are enhanced when the number of carriers increases. The interaction between photogenerated carriers and MA ions supports the idea of screening via formation of polarons, facilitating the appearance of long carrier lifetimes in these compounds. The next step concerning μ^+SR would be a controlled, laser illumination with measurements in various crystallographic directions to access detailed diffusion information of all ionic species. Finally, muonium formation was observed that opens up the possibility to study hydrogen kinematics in the title compounds in future μ^+SR studies.

5. Experimental Section

Single crystals of $MAPbBr_3$ and $MAPbCl_3$ were grown according to Ref. [66]. Differential scanning calorimetry (DSC) and temperature-modulated DSC were performed on both crystals to macroscopically identify the structural transition and molecular fluctuation occurrences (see Figure S1.1, Supporting Information).

The μ^+SR measurements were conducted at the pulsed surface muon beam-line EMU at ISIS.[67] Rectangular single crystal pieces were aligned on Ag holders and mounted in the fly-pass configuration. The crystals were wrapped in Ag foil for measurements in the dark. For measurements in

an illuminated environment a transparent, 10 μm Mylar film was used instead, and the sample was mounted at 45° (Figure 2b) making it possible to accommodate both light and muon pulses. The samples were measured in ZF, LF, and TF geometry, where transverse and longitudinal magnetic field refers to the applied field direction with respect to the initial muon spin polarization. For the measurements under illumination, a NISSIN SX-100 XENON flash lamp was used with a spectral distribution of 250-1020 nm covering the reported absorption spectra of these samples in the ultraviolet and visible range.[11,68–70] The flash lamp was operated with intensity 1.52 mJ/pulse, but pulsed at 50 Hz in order to minimize the temperature increase caused by light irradiation. The relative intensity was stable at ≈ 20% between 750–370 nm and decreased below 370 nm. Spectra were recorded during two periods of 10 s, light on and off, with 500 muon pulses being recorded in each state. The 80 ns wide muon pulses, each containing a few hundred muons, were implanted in the sample at 50 Hz, synchronously with the light on and off cycle. Data acquisition alternated continuously between the two states for the duration of the run. The software package *musrfit* was used to analyze the data.[71]

The electrostatic potential of the compounds was calculated with DFT, determined via a self consistent run using the pseudopotential-based plane-wave method as implemented in Quantum Espresso.[72] The pseudopotentials are based on [73, 74]. This calculation was performed for all crystal symmetries the system exhibits between 100 – 300 K; orthorhombic, tetragonal, and cubic structures. The electrostatic minimum was asserted to be the muon site (Figure 1b). It was noted that local distortion due to the implanted muon was not considered.

Supporting Information

Supporting Information is available from the Wiley Online Library or from the author.

Acknowledgements

The authors thank Dr. Nami Matsubara for support at the experiment. This research was supported by the European Commission through a Marie Skłodowska-Curie Action and the Swedish Research Council - VR (Dnr. 2014-6426 and 2016-06955), as well as the Carl Tryggers Foundation for Scientific Research (CTS-18:272). J.S. acknowledged support from Japan Society for the Promotion Science (JSPS) KAKENHI Grant nos. JP18H01863, JP20K21149, and JP23H01840. P.K.N. acknowledged support from the Department of Atomic Energy, Government of India, under project identification no. RTI 4007, and Swarna Jayanti Fellowship, DST, India. O.K.F. acknowledged funding from the Swedish Research Council (VR) through the Postdoc International grant (Dnr. 2022-06217) and the Foundation Blanceflor 2023 fellow scholarship. Y.S. acknowledged funding from the Swedish Research Council (VR) through a Starting Grant (Dnr. 2017-05078) and the Knut and Alice Wallenberg Foundation through the grant 2021.0150. E.N is funded by the SSF-Swedness grant SNP21-0004. Y.S. and K.P. were funded by the Area of Advance - Material Sciences from Chalmers University of Technology. The measurements presented in the supporting information were performed in part at the Chalmers Material Analysis Laboratory (CMAL) and the Material Physics Division. Images involving crystal structure were made with the VESTA software.[75]

Conflict of Interest

The authors declare no conflict of interest.

Data Availability Statement

The data that support the findings of this study are available from the corresponding author upon reasonable request.

Keywords

ion dynamics, organic-inorganic hybrid perovskite, muon spin spectroscopy, structural stability

Received: October 16, 2023
Revised: November 27, 2023
Published online: January 10, 2024

[1] D. M. Chapin, C. S. Fuller, G. L. Pearson, *J. Appl. Phys.* **1954**, *25*, 676.
[2] M. Grätzel, *Nat. Mater.* **2014**, *13*, 838.
[3] Best research cell efficiency chart - nrel, https://www.nrel.gov/pv/assets/pdfs/best-research-cell-efficiencies.pdf, (accessed: August **2023**).
[4] W. Shen, Y. Zhao, F. Liu, *Front. Energy* **2023**, *17*, 9.
[5] (Eds.: N. S. Arul, V. D. Nithya), *Revolution of Perovskite*, Springer Singapore, Singapore **2020**.
[6] (Ed.: H. Fujiwara), *Hybrid Perovskite Solar Cells*, Wiley, New York **2021**.
[7] A. Poglitsch, D. Weber, *J. Chem. Phys.* **1987**, *87*, 6373.
[8] W.-H. Li, C.-H. Lee, T.-Y. Ling, M.-H. Ma, P.-C. Wei, J.-H. He, C.-M. Wu, J.-C. Peng, G. Xu, Y. Zhao, J. W. Lynn, *Phys. Rev. Mater.* **2021**, *5*, 025401.
[9] C. A. López, M. V. Martínez-Huerta, M. C. Alvarez-Galván, P. Kayser, P. Gant, A. Castellanos-Gomez, M. T. Fernández-Díaz, F. Fauth, J. A. Alonso, *Inorg. Chem.* **2017**, *56*, 14214.
[10] K.-H. Wang, L.-C. Li, M. Shellaiah, K. W. Sun, *Sci. Rep.* **2017**, *7*, 1.
[11] H.-P. Hsu, L.-C. Li, M. Shellaiah, K. W. Sun, *Sci. Rep.* **2019**, *9*, 1.
[12] E. L. Unger, L. Kegelmann, K. Suchan, D. Sörell, L. Korte, S. Albrecht, *J. Mater. Chem. A* **2017**, *5*, 11401.
[13] Y. Yang, Y. Yan, M. Yang, S. Choi, K. Zhu, J. M. Luther, M. C. Beard, *Nat. Commun.* **2015**, *6*, 1.
[14] N. K. Kumawat, A. Dey, A. Kumar, S. P. Gopinathan, K. L. Narasimhan, D. Kabra, *ACS Appl. Mater. Interfaces* **2015**, *7*, 13119.
[15] D. Shi, V. Adinolfi, R. Comin, M. Yuan, E. Alarousu, A. Buin, Y. Chen, S. Hoogland, A. Rothenberger, K. Katsiev, Y. Losovyj, X. Zhang, P. A. Dowben, O. F. Mohammed, E. H. Sargent, O. M. Bakr, *Science* **2015**, *347*, 519.
[16] J. Xing, Y. Zou, C. Zhao, Z. Yu, Y. Shan, W. Kong, X. Zheng, X. Li, W. Yu, C. Guo, *Mater. Today Phys.* **2020**, *14*, 100240.
[17] Y. Yamada, T. Yamada, L. Q. Phuong, N. Maruyama, H. Nishimura, A. Wakamiya, Y. Murata, Y. Kanemitsu, *J. Am. Chem. Soc.* **2015**, *137*, 10456.
[18] H. Li, Z. Zhang, W. Jiang, C. Zhao, H. Di, J. Ren, B. Ou, Y. Xiong, F. Liao, Y. Zhao, *J. Mater. Chem. A* **2023**, *11*, 16201.
[19] S. D. Stranks, G. E. Eperon, G. Grancini, C. Menelaou, M. J. P. Alcocer, T. Leijtens, L. M. Herz, A. Petrozza, H. J. Snaith, *Science* **2013**, *342*, 341.
[20] S. Govinda, B. P. Kore, M. Bokdam, P. Mahale, A. Kumar, S. Pal, B. Bhattacharyya, J. Lahnsteiner, G. Kresse, C. Franchini, A. Pandey, D. D. Sarma, *J. Phys. Chem. Lett.* **2017**, *8*, 4113.
[21] T. Chen, B. J. Foley, B. Ipek, M. Tyagi, J. R. D. Copley, C. M. Brown, J. J. Choi, S.-H. Lee, *Phys. Chem. Chem. Phys.* **2015**, *17*, 31278.
[22] H. Zhu, K. Miyata, Y. Fu, J. Wang, P. P. Joshi, D. Niesner, K. W. Williams, S. Jin, X.-Y. Zhu, *Science* **2016**, *353*, 1409.
[23] J. Sugiyama, K. Mukai, Y. Ikedo, H. Nozaki, M. Månsson, I. Watanabe, *Phys. Rev. Lett.* **2009**, *103*, 147601.
[24] I. McClelland, B. Johnston, P. J. Baker, M. Amores, E. J. Cussen, S. A. Corr, *Annu. Rev. Mater. Res.* **2020**, *50*, 371.
[25] A. Koda, H. Okabe, M. Hiraishi, R. Kadono, K. A. Dagnall, J. J. Choi, S.-H. Lee, *Proc. Natl. Acad. Sci.* **2022**, *119*, 4.
[26] J. Sugiyama, H. Nozaki, I. Umegaki, K. Mukai, K. Miwa, S. Shiraki, T. Hitosugi, A. Suter, T. Prokscha, Z. Salman, J. S. Lord, M. Månsson, *Phys. Rev. B* **2015**, *92*, 1.

[27] O. K. Forslund, R. Toft-Petersen, D. Vaknin, N. van Well, M. Telling, Y. Sassa, J. Sugiyama, M. Månsson, F. Juranyi, *arXiv* **2021**, *2111*, 11941.
[28] P. D. De Reotier, A. Yaouanc, *J. Phys.: Condens. Matter* **1997**, *9*, 9113.
[29] R. S. Hayano, Y. J. Uemura, J. Imazato, N. Nishida, T. Yamazaki, R. Kubo, *Phys. Rev. B* **1979**, *20*, 850.
[30] J. H. V. Vleck, *Phys. Rev.* **1948**, *74*, 1168.
[31] A. L. Yaouanc, P. D. de Réotier, *Muon spin rotation, relaxation, and resonance: Applications to Condensed Matter*, Oxford University Press, Oxford **2011**.
[32] I. Swainson, R. Hammond, C. Soullière, O. Knop, W. Massa, *J. Solid State Chem.* **2003**, *176*, 97.
[33] I. P. Swainson, *Acta Crystallogr., Sect. B: Struct. Sci.* **2005**, *61*, 616.
[34] D. W. Ferdani, S. R. Pering, D. Ghosh, P. Kubiak, A. B. Walker, S. E. Lewis, A. L. Johnson, P. J. Baker, M. S. Islam, P. J. Cameron, *Energy Environ. Sci.* **2019**, *12*, 2264.
[35] O. K. Forslund, H. Ohta, K. Kamazawa, S. L. Stubbs, O. Ofer, M. Månsson, C. Michioka, K. Yoshimura, B. Hitti, D. Arseneau, G. D. Morris, E. J. Ansaldo, J. H. Brewer, J. Sugiyama, *Phys. Rev. B* **2020**, *102*, 184412.
[36] R. Wasylishen, O. Knop, J. Macdonald, *Solid State Commun.* **1985**, *56*, 581.
[37] O. Knop, R. E. Wasylishen, M. A. White, T. S. Cameron, M. J. M. V. Oort, *Can. J. Chem.* **1990**, *68*, 412.
[38] G. M. Bernard, R. E. Wasylishen, C. I. Ratcliffe, V. Terskikh, Q. Wu, J. M. Buriak, T. Hauger, *J. Phys. Chem. A* **2018**, *122*, 1560.
[39] I. P. Swainson, C. Stock, S. F. Parker, L. Van Eijck, M. Russina, J. W. Taylor, *Phys. Rev. B* **2015**, *92*, 10.
[40] D. Y. Park, Y. H. Shin, Y. Kim, *J. Phys. Chem. C* **2023**, *127*, 21235.
[41] Q. Xu, T. Eguchi, H. Nakayama, N. Nakamura, M. Kishita, *Z. Naturforsch., A* **1991**, *46*, 240.
[42] Y. Furukawa, D. Nakamura, *Z. Naturforsch., A* **1989**, *44*, 1122.
[43] G. Schuck, F. Lehmann, J. Ollivier, H. Mutka, S. Schorr, *J. Phys. Chem. C* **2019**, *123*, 11436.
[44] M. Songvilay, Z. Wang, V. G. Sakai, T. Guidi, M. Bari, Z.-G. Ye, G. Xu, K. L. Brown, P. M. Gehring, C. Stock, *Phys. Rev. Mater.* **2019**, *3*, 12.
[45] F. El-Mellouhi, E. T. Bentria, A. Marzouk, S. N. Rashkeev, S. Kais, F. H. Alharbi, *npj Comput. Mater.* **2016**, *2*, 1.
[46] H. Fujiwara, *Hybrid perovskite solar cells: Characteristics and Operation*, Wiley-VCH, Weinheim **2022**.
[47] K. L. Svane, A. C. Forse, C. P. Grey, G. Kieslich, A. K. Cheetham, A. Walsh, K. T. Butler, *J. Phys. Chem. Lett.* **2017**, *8*, 6154.
[48] J. M. Frost, A. Walsh, *Acc. Chem. Res.* **2016**, *49*, 528.
[49] D. Ghosh, P. Walsh Atkins, M. S. Islam, A. B. Walker, C. Eames, *ACS Energy Lett.* **2017**, *2*, 2424.
[50] R. García-Rodríguez, D. Ferdani, S. Pering, P. J. Baker, P. J. Cameron, *J. Mater. Chem. A* **2019**, *7*, 22604.
[51] N. Onoda-Yamamuro, T. Matsuo, H. Suga, *J. Phys. Chem. Solids* **1992**, *53*, 935.
[52] H. R. Jung, Y. Cho, W. Jo, *Adv. Opt. Mater.* **2022**, *10*, 2102175.
[53] H. Zhu, K. Miyata, Y. Fu, J. Wang, P. P. Joshi, D. Niesner, K. W. Williams, S. Jin, X.-Y. Zhu, *Science* **2016**, *353*, 1409.
[54] T. Chen, W.-L. Chen, B. J. Foley, J. Lee, J. P. C. Ruff, J. Y. P. Ko, C. M. Brown, L. W. Harriger, D. Zhang, C. Park, M. Yoon, Y.-M. Chang, J. J. Choi, S.-H. Lee, *Proc. Natl. Acad. Sci.* **2017**, *114*, 7519.
[55] Y. Chen, H. T. Yi, X. Wu, R. Haroldson, Y. N. Gartstein, Y. I. Rodionov, K. S. Tikhonov, A. Zakhidov, X. Y. Zhu, V. Podzorov, *Nat. Commun.* **2016**, *7*, 1.
[56] J. Sugiyama, O. K. Forslund, E. Nocerino, N. Matsubara, K. Papadopoulos, Y. Sassa, S. P. Cottrell, A. D. Hillier, K. Ishida, M. Månsson, J. H. Brewer, *Phys. Rev. Res.* **2020**, *2*, 033161.
[57] R. A. Kerner, B. P. Rand, *J. Phys. Chem. Lett.* **2017**, *9*, 132.
[58] C. Boekema, K. C. Chan, R. L. Lichti, A. B. Denison, D. W. Cooke, R. H. Heffner, R. L. Hutson, M. E. Schillaci, *Hyperfine Interact.* **1986**, *32*, 667.
[59] S. Cox, J. Lord, S. Cottrell, J. Gil, H. Alberto, A. Keren, D. Prabhakaran, R. Scheuermann, A. Stoykov, *J. Phys.: Condens. Matter* **2006**, *18*, 1061.
[60] S. J. Blundell, T. Lancaster, P. J. Baker, W. Hayes, F. L. Pratt, T. Atake, D. S. Rana, S. K. Malik, *Phys. Rev. B* **2008**, *77*, 094424.
[61] O. K. Forslund, *JPS Conf. Proc.* **2018**, *21*, 011066.
[62] V. G. Storchak, D. G. Eshchenko, J. H. Brewer, *J. Phys.: Condens. Matter* **2004**, *16*, S4761.
[63] Y. Liang, X. Cui, F. Li, C. Stampfl, S. P. Ringer, R. Zheng, *J. Phys. Chem. C* **2022**, *126*, 1721.
[64] S. F. J. Cox, *Rep. Prog. Phys.* **2009**, *72*, 116501.
[65] R. Kadono, A. Matsushita, R. M. Macrae, K. Nishiyama, K. Nagamine, *Phys. Rev. Lett.* **1994**, *73*, 2724.
[66] P. K. Nayak, D. T. Moore, B. Wenger, S. Nayak, A. A. Haghighirad, A. Fineberg, N. K. Noel, O. G. Reid, G. Rumbles, P. Kukura, K. A. Vincent, H. J. Snaith, *Nat. Commun.* **2016**, *7*, 1.
[67] S. Giblin, S. Cottrell, P. King, S. Tomlinson, S. Jago, L. Randall, M. Roberts, J. Norris, S. Howarth, Q. Mutamba, N. Rhodes, F. Akeroyd, *Nucl. Instrum. Methods Phys. Res. A: Accel. Spectrom. Detect. Assoc. Equip.* **2014**, *751*, 70.
[68] K. H. Wei, B. J. Chen, L. B. Zhang, H. R. Zhu, S. H. Fan, *Laser Phys. Lett.* **2022**, *19*, 056003.
[69] Z. Zuo, J. Ding, Y. Zhao, S. Du, Y. Li, X. Zhan, H. Cui, *J. Phys. Chem. Lett.* **2017**, *8*, 684.
[70] G. Maculan, A. D. Sheikh, A. L. Abdelhady, M. I. Saidaminov, M. A. Haque, B. Murali, E. Alarousu, O. F. Mohammed, T. Wu, O. M. Bakr, *J. Phys. Chem. Lett.* **2015**, *6*, 3781.
[71] A. Suter, B. Wojek, *Phys. Procedia* **2012**, *30*, 69.
[72] P. Giannozzi, O. Andreussi, T. Brumme, O. Bunau, M. B. Nardelli, M. Calandra, R. Car, C. Cavazzoni, D. Ceresoli, M. Cococcioni, N. Colonna, I. Carnimeo, A. D. Corso, S. de Gironcoli, P. Delugas, R. A. DiStasio, A. Ferretti, A. Floris, G. Fratesi, G. Fugallo, R. Gebauer, U. Gerstmann, F. Giustino, T. Gorni, J. Jia, M. Kawamura, H.-Y. Ko, A. Kokalj, E. Küçükbenli, M. Lazzeri, et al., *J. Phys.: Condens. Matter* **2017**, *29*, 465901.
[73] K. Lejaeghere, G. Bihlmayer, T. Björkman, P. Blaha, S. Blügel, V. Blum, D. Caliste, I. E. Castelli, S. J. Clark, A. D. Corso, S. de Gironcoli, T. Deutsch, J. K. Dewhurst, I. D. Marco, C. Draxl, M. Dułak, O. Eriksson, J. A. Flores-Livas, K. F. Garrity, L. Genovese, P. Giannozzi, M. Giantomassi, S. Goedecker, X. Gonze, O. Grånäs, E. K. U. Gross, A. Gulans, F. Gygi, D. R. Hamann, P. J. Hasnip, et al., *Science* **2016**, *351*, aad3000.
[74] G. Prandini, A. Marrazzo, I. E. Castelli, N. Mounet, N. Marzari, *npj Comput. Mater.* **2018**, *4*, 72.
[75] K. Momma, F. Izumi, *J. Appl. Crystallogr.* **2011**, *44*, 1272.